Supporting Information for

Co-organisation of ionic liquids with amphiphilic diethanolamines: construction of 3D continuous ionic nanochannels through the induction of liquid-crystalline bicontinuous cubic phases

Takahiro Ichikawa, Masafumi Yoshio, Satomi Taguchi, Junko Kagimoto, Hiroyuki Ohno and Takashi Kato*

Contents

1. General Procedures and Materials.

General Procedures. ^{1}H NMR and ^{13}C NMR spectra were obtained on a JEOL JNM-LA400 at 400 and 100 MHz in $CDCl_3$, respectively. Chemical shifts of ^{1}H and ^{13}C NMR signals were quoted to $(CH_3)_4Si$ ($\delta = 0.00$) and $CDCl_3$ ($\delta = 77.0$) as internal standards, respectively. Elemental analyses were carried out on a Yanaco MT-6 CHN autocorder and an Exeter Analytical CE440 instrument. The thermal properties of the materials were examined by a DSC using a Netzsch DSC204 *Phoenix*. The heating and cooling rates were 10 °C min^{-1}. Transition temperatures were taken at the onset of the transition peaks. A polarising optical microscope Olympus BX51 equipped with a Mettler FP82HT hot stage was used for visual observation. Wide-angle X-ray diffraction (WAXD) patterns were obtained using a Rigaku RINT-2500 diffractometer with Cu Kα radiation.

Materials. All chemical reagents and solvents were obtained from commercial sources and used without purification. All reactions were carried out under an argon atmosphere in anhydrous solvents.

Measurement of Ionic Conductivities. Temperature dependence of the ionic conductivities was measured in the heating process by the alternating current impedance method using a Schlumberger Solartron 1260 impedance analyzer (frequency range: 10 Hz-10 MHz, applied voltage: 0.3 V) equipped with a temperature controller. The cooling rate was fixed to 2 K min^{-1}. Ionic conductivities were practically calculated to be the product of $1/R_b$ (Ω^{-1}) times cell constants (cm^{-1}) of the comb-shaped gold electrodes, which were calibrated with KCl aqueous solution (1.00 mmol L^{-1}) as a standard conductive solution. The impedance data (Z) were modeled as a connection of two RC circuits in series.

2. Synthesis

Synthesis of *N*-{3-[*N'*, *N'*-bis(2-hydroxyethyl)aminopropyl]}-3,4- Didodecyloxybenzoylamide 1, *N*-{3-[*N'*, *N'*-bis(2-hydroxyethyl)aminopropyl]}-3,5- Didodecyloxybenzoylamide 2, and *N*-{3-[*N'*, *N'*-bis(2-hydroxyethyl)aminopropyl]}-3,4,5- Didodecyloxybenzoylamide 3.

The synthetic pathways used to obtain compounds **1-3** are shown in **Scheme S1**. Methyl-3,4-dihydroxybenzoate, methyl-3,4-dihydroxybenzoate, and methyl-3,4,5-trihydroxy benzoate were etherified with 1-bromododecane in the presence of potassium carbonate (K_2CO_3) in *N*,*N*-dimethylformamide (DMF) to yield methyl-3,4-didodecyloxybenzoates **7a**, methyl-3,5-didodecyloxybenzoates **7b**, and methyl-3,4,5-trisdodecyloxybenzoates **7c**, respectively. Subsequent hydrolysis of the resulting compounds **7a-c** gave benzoic acid derivatives **8a-c**. Finally, amphiphilic diethanolamine molecules **1-3** were prepared by amidation reactions of *N*-(3-aminopropyl) diethanolamine and benzoic acid derivatives **8a-c**.

Scheme S1. Synthesis of amphiphilic diethanolamine molecules **1-3**.

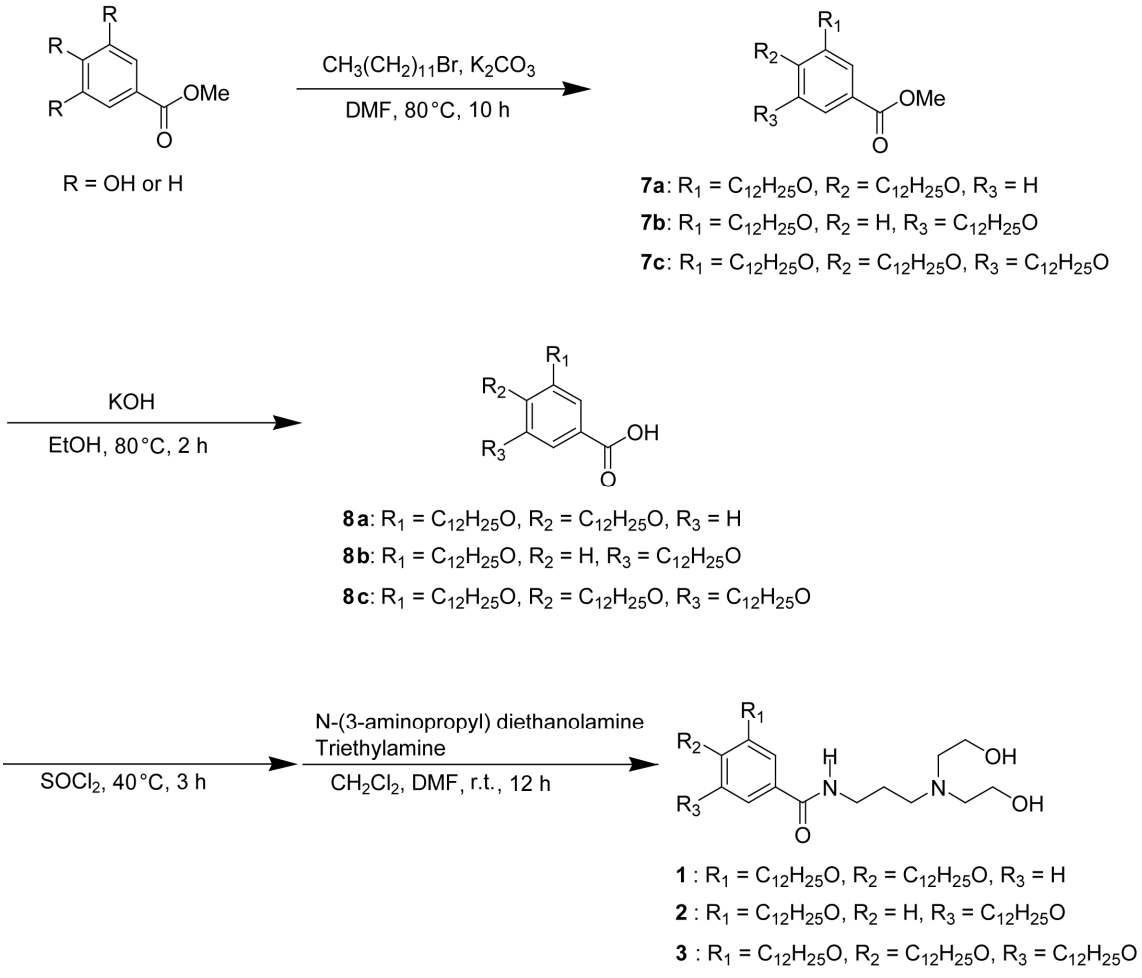

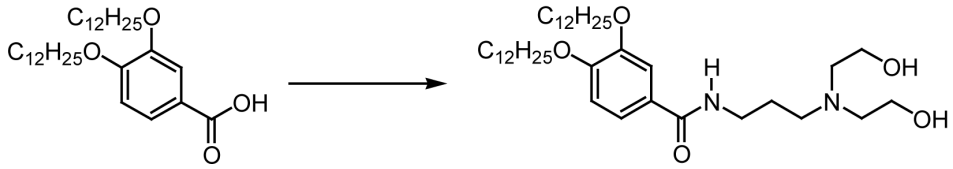

1

3,4-Didodecyloxybenzoic acid (3.0 g, 6.11 mmol) dissolved in thionyl chloride ($SOCl_2$) (10 mL) was refluxed for 3 h with stirring before the excess of $SOCl_2$ was removed under reduced pressure. The residue was dissolved in dry dichloromethane (CH_2Cl_2) (20 mL), and the flask was cooled to 0 °C by an ice bath. The obtained solution was then added dropwise to a solution of *N*-(3-aminopropyl) diethanolamine (5.0 g, 30.8 mmol) and triethylamine (5 mL) in dry dimethyl formamide (DMF) (20 mL) at 0 °C. The resulting mixture was stirred overnight at room temperature. The reaction mixture was extracted three times with ethyl acetate and washed with water three times. The resulting organic phase was dried over anhydrous $MgSO_4$, filtered through a pad of celite, and concentrated under reduced pressure. The crude product was purified by flash column chromatography (silica gel, eluent CH_2Cl_2/methanol = 15/1) to give *N*-{3-[*N'*, *N'*-bis(2-hydroxyethyl)aminopropyl]}-3,4-didodecyloxybenzoylamide 2.1 g (54 %) as a white solid.

^{1}H NMR (400 MHz): δ = 7.42 (d, *J* = 2.0 Hz, 1H), 7.32 (dd, *J* = 8.3, 2.0 Hz, 1H), 7.03 (t, *J* = 5.9 Hz, 1H), 6.82 (d, *J* = 8.8 Hz, 1H), 4.01 (m, 4H), 3.60 (t, *J* = 4.9 Hz, 4H), 3.53 (m, 2H), 2.57 (m, 6H), 1.78 (m, 6H), 1.47-1.26 (m, 36 H), 0.88 (t, *J* = 6.8 Hz, 6H), ^{13}C NMR (100 MHz): δ= 167.63, 151.79, 148.75, 126.74, 119.65, 112.67, 112.11, 69.23, 69.00, 59.53, 56.13, 51.73, 37.66, 31.88, 29.68, 29.66, 29.61, 29.58, 29.40, 29.39, 29.33, 29.19, 29.09, 27.02, 25.98, 25.96, 22.64 14.08.

IR (KBr): ν = 3254, 2917, 2849, 1633, 1546, 1513, 1468, 1391, 1321, 1270, 1223, 1153, 1131, 1056, 873, 822, 721 cm^{-1}.
MS (MALDI-TOF): calcd. for [M + H]$^+$, 634.53. Found: 635.64.
Elemental analysis calcd (%) for $C_{44}H_{72}O_5$: C, 71.88; H, 11.11, N, 4.41. Found: C, 71.88; H, 11.13, N, 4.58.

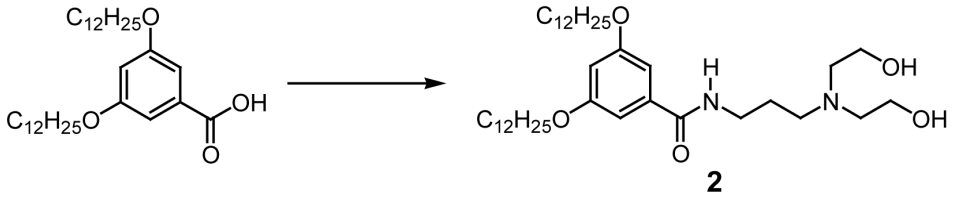

2

3,5-Didodecyloxybenzoic acid (3.0 g, 6.11 mmol) dissolved in $SOCl_2$ (10 mL) was refluxed for 3 h with stirring before the excess of $SOCl_2$ was removed under reduced pressure. The residue was dissolved in dry CH_2Cl_2 (20 mL), and the flask was cooled to 0 °C by an ice bath. The obtained solution was then added dropwise to a solution of *N*-(3-aminopropyl) diethanolamine (5.0 g, 30.8 mmol) and triethylamine (5 mL) in dry DMF (20 mL) at 0 °C. The resulting mixture was stirred overnight at room temperature. The reaction mixture was extracted three times with ethyl acetate and washed with water three times. The resulting organic phase was dried over anhydrous $MgSO_4$, filtered through a pad of celite, and concentrated under reduced pressure. The crude product was purified by flash column chromatography (silica gel, eluent CH_2Cl_2/methanol = 15/1) to give *N*-{3-[*N'*, *N'*-bis(2-hydroxyethyl)aminopropyl]}-3,5-didodecyloxybenzoylamide 1.8 g (46 %) as a white solid.

^{1}H NMR (400 MHz): δ = 6.88 (d, *J* = 2.4 Hz, 2H), 6.70 (t, *J* =5.9 Hz, 1H), 6.55 (t, *J* = 1.9 Hz, 1H), 3.96 (t, *J* = 6.6 Hz, 4H), 3.63 (t, *J* = 4.9 Hz, 4H), 3.57 (dt, *J* = 6.4, 6.3 Hz, 2H), 2.63 (t, *J* = 5.1 Hz, 4H), 2.60 (t, *J* = 6.4 Hz, 2H), 1.76 (m, 6H), 1.44-1.26 (m, 36 H), 0.88 (t, *J* = 6.8 Hz, 6H), ^{13}C NMR (100 MHz): δ= 166.92, 152.80, 137.33, 135.50, 130.88, 124.65, 114.58, 107.98, 73.46, 69.12, 52.09, 32.54, 31.93, 30.31, 29.73, 29.72, 29.70, 29.68, 29.55, 29.44, 29.38, 29.30, 29.27, 29.17, 29.15, 26.04, 22.69, 14.11.

IR (KBr): ν = 3274, 3211, 3074, 2914, 2851, 1629, 1593, 1556, 1767, 1439, 1383, 1330, 1087, 1035, 988, 897, 858, 787, 757, 736 cm^{-1}.

MS (MALDI-TOF): calcd. for $[M + H]^+$, 634.53. Found: 635.67.

Elemental analysis calcd (%) for $C_{44}H_{72}O_5$: C, 71.88; H, 11.11, N, 4.41. Found: C, 71.92; H, 11.11, N, 4.54.

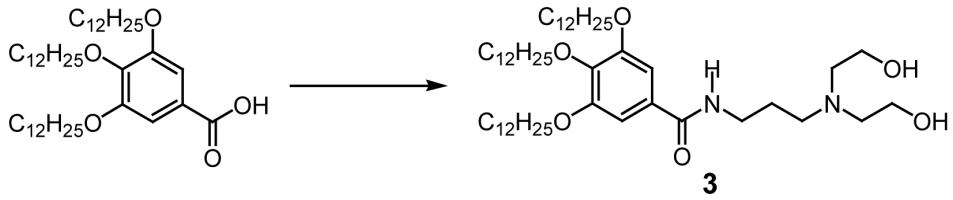

3

3,4,5-trisdodecyloxybenzoic acid (3.0 g, 4.44 mmol) dissolved in $SOCl_2$ (10 mL) was refluxed for 3 h with stirring before the excess of $SOCl_2$ was removed under reduced pressure. The residue was dissolved in dry CH_2Cl_2 (20 mL), and the flask was cooled to 0 °C by an ice bath. The obtained solution was then added dropwise to a solution of *N*-(3-aminopropyl) diethanolamine (4.0 g, 24.7 mmol) and triethylamine (5 mL) in dry DMF (20 mL) at 0 °C. The resulting mixture was stirred overnight at room temperature. The reaction mixture was extracted three times with ethyl acetate and washed with water three times. The resulting organic phase was dried over anhydrous $MgSO_4$, filtered through a pad of celite, and concentrated under reduced pressure. The crude product was purified by flash column chromatography (silica gel, eluent CH_2Cl_2/methanol = 15/1) to give *N*-{3-[*N'*, *N'*-bis(2-hydroxyethyl)aminopropyl]}-3,4,5-trisdodecyloxybenzoylamide 2.4 g (66 %) as a white solid.

^{1}H NMR (400 MHz): δ = 7.00 (s, 2H), 6.80 (t, *J* =5.9 Hz, 1H), 3.98 (m, 6H), 3.63 (t, *J* = 5.1 Hz, 4H), 3.55 (dt, *J* = 6.4, 6.3 Hz, 2H), 2.63 (m, 6H), 1.76 (m, 8H), 1.47-1.26 (m, 54 H), 0.88 (t, *J* = 6.8 Hz, 9H), ^{13}C NMR (100 MHz): δ= 167.73, 152.91, 140.81, 129.24, 105.57, 7340, 69.16, 59.40, 56.09, 51.64, 37.71, 31.87, 30.28, 29.71, 29.67, 29.64, 29.62, 29.55, 29.40, 29.32, 26.87, 26.07, 26.03, 22.64, 14.06.

IR (KBr): ν = 3399, 3265, 3086, 2919, 2850, 1633, 1580, 1542, 1501, 1467, 1427, 1386, 1340, 1238, 1123, 1038, 843, 721 cm^{-1}.
MS (MALDI-TOF): calcd. for $[M + H]^+$, 818.71. Found: 819.73.
Elemental analysis calcd (%) for $C_{44}H_{72}O_5$: C, 73.30; H, 11.56, N, 3.42. Found: C, 73.13; H, 11.51, N, 3.57.

3. POM, DSC and XRD Results for Individual Compounds 1-3

3.1. POM, DSC and XRD Results for Individual Compound **1**

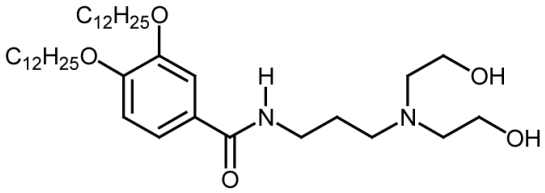

1

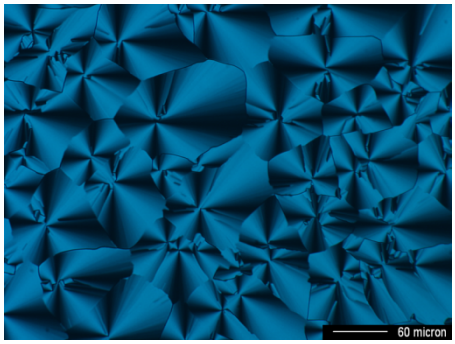

Figure S1. Polarising optical microscopic image of **1** in the Col_{H2} phase at 50 °C.

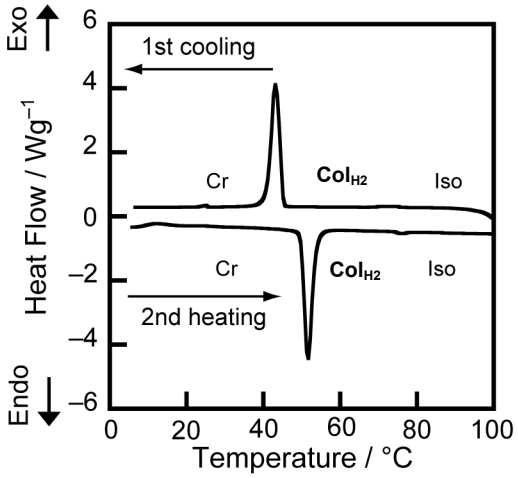

Figure S2. DSC thermograms of **1**.

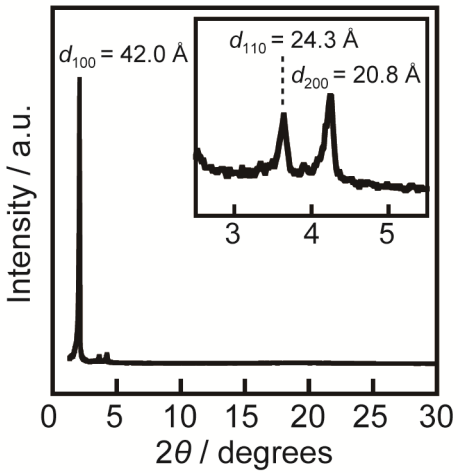

Figure S3. Wide-angle X-ray diffraction pattern of **1** in the Col_{H2} phase at 50 °C.

3.2. POM, DSC and XRD Results for Individual Compound **2**

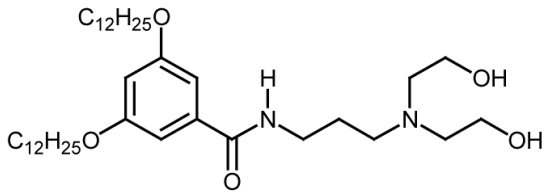

2

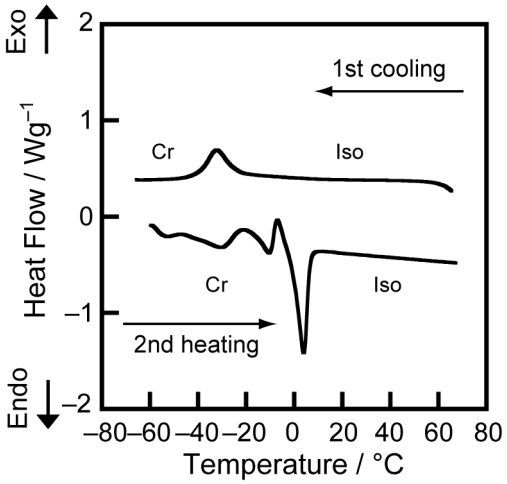

Figure S4. DSC thermograms of **2**.

3.3. POM, DSC and XRD Results for Individual Compound **3**

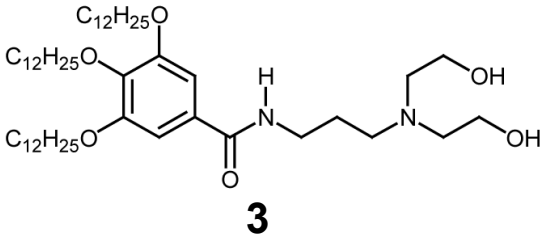

3

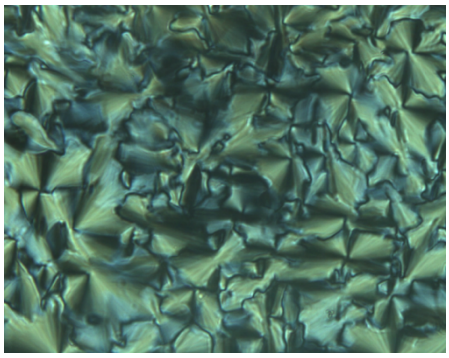

Figure S5. Polarising optical microscopic image of **3** in the Col_{H2} phase at 50 °C.

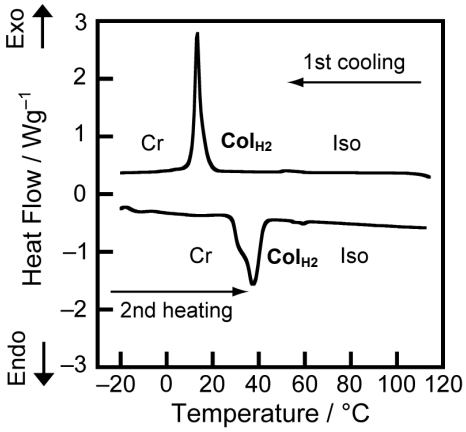

Figure S6. DSC thermograms of **3**.

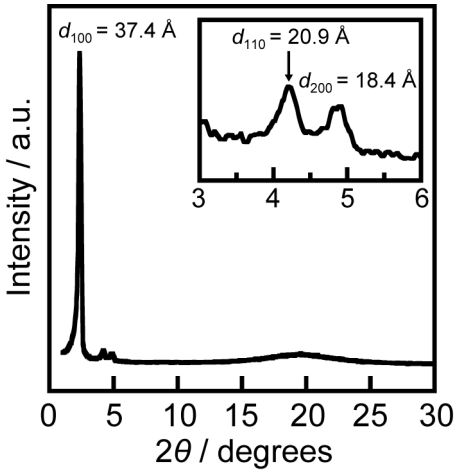

Figure S7. Wide-angle X-ray diffraction pattern of **3** in the Col_{H2} phase at 50 °C.

3.4. Table of thermal properties of Compounds **1-3**

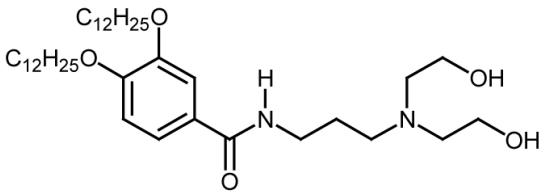

1

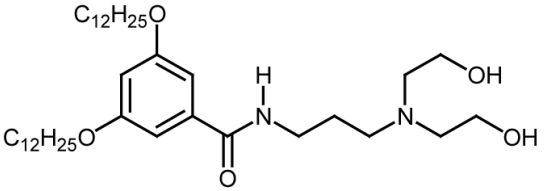

2

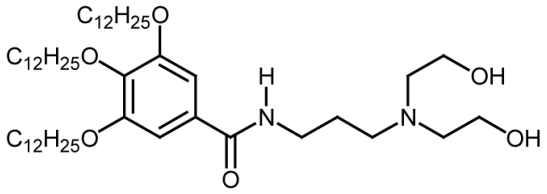

3

Table S1. Thermal properties of compounds **1-3**

Compound	Phase transition behaviour / °C[a]				
1	Cr	50 (38)	Col_{H2}	74 (0.43)	Iso
2	Cr	0 (19)	Iso		
3	Cr	37 (45)	Col_{H2}	58 (0.24)	Iso

Cr, crystalline; Col_{H2}, hexagonal columnar; Iso, isotropic. [a]Transition temperatures (°C) and enthalpy changes (kJ mol^{-1}, in parentheses) are determined by DSC on the second heating

4. POM, DSC and XRD Results for Mixtures of 1-3 with Ionic Liquids 4-5

4.1. POM, DSC and XRD Results for Mixtures **1**/**4**

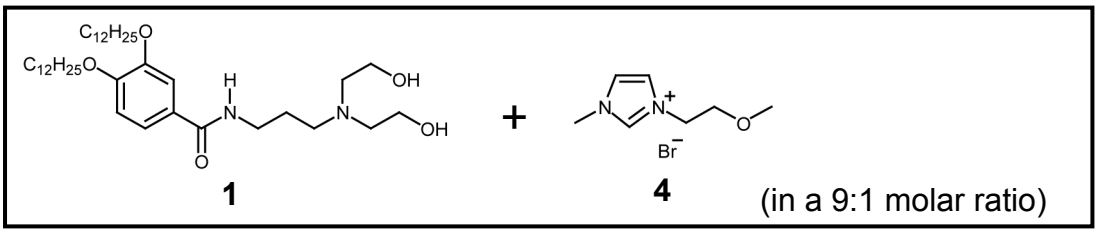

Figure S8. Polarising optical micrograph of mixture **1**/**4** in a 9:1 molar ratio in the Cub_{V2} at 55 °C.

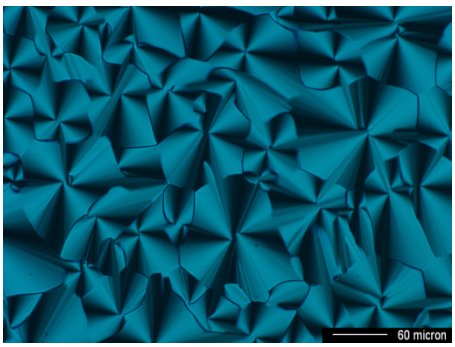

Figure S9. Polarising optical micrograph of mixture **1**/**4** in a 9:1 molar ratio in the Col_{H2} at 60 °C.

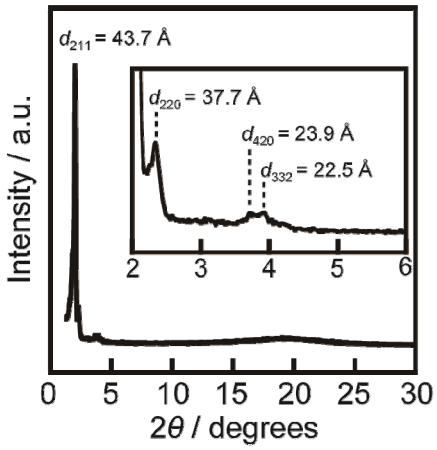

Figure S10. Wide-angle X-ray diffraction pattern of mixture **1**/**4** in a 9:1 molar ratio in the Cub_{V2} at 50 °C.

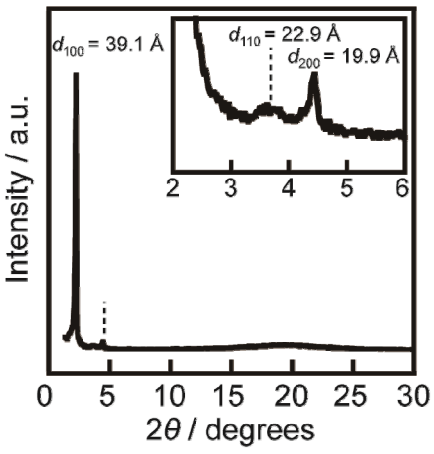

Figure S11. Wide-angle X-ray diffraction pattern of mixture **1**/**4** in a 9:1 molar ratio in the Col_{H2} at 65 °C.

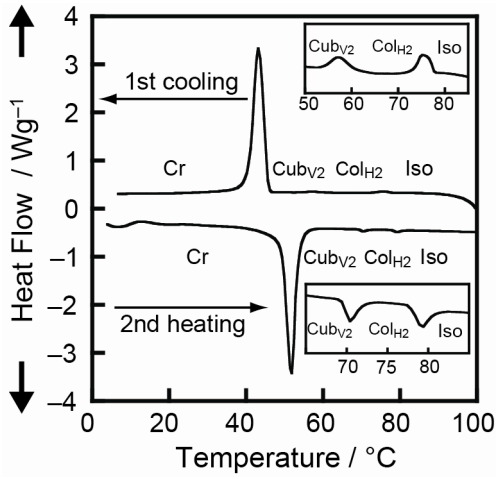

Figure S12. DSC thermograms of mixture **1**/**4** in a 9:1 molar ratio.

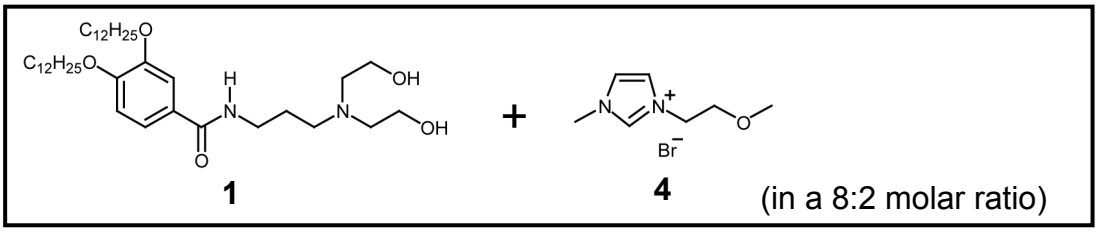

Figure S13. Polarising optical micrograph of mixture **1**/**4** in an 8:2 molar ratio in the Cub$_{V2}$ phase at 55 °C.

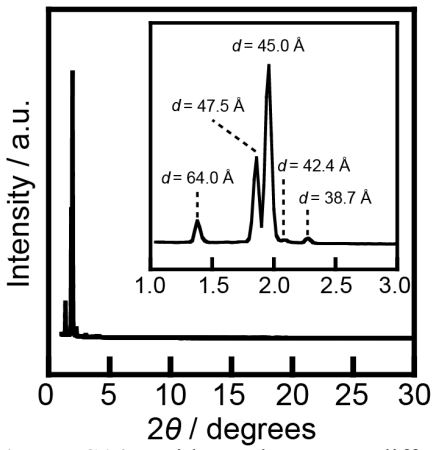

Figure S14. Wide-angle X-ray diffraction pattern of mixture **1**/**4** in an 8:2 molar ratio in the Cub$_{V2}$ phase at 55 °C.

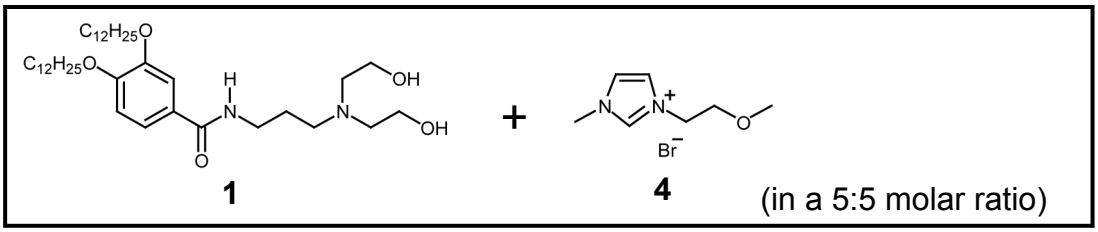

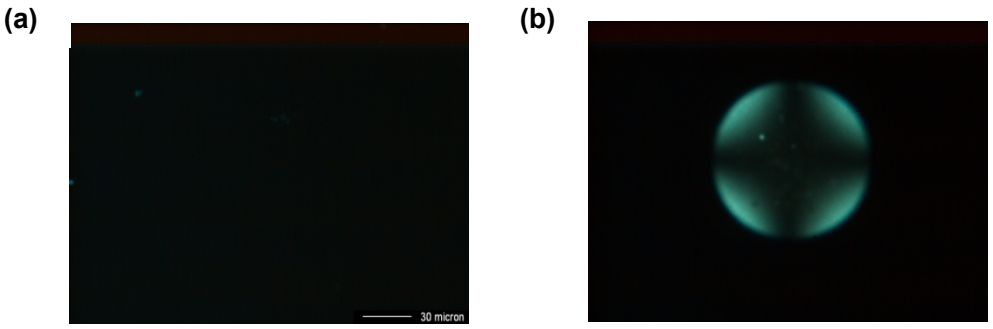

Figure S15. (a) Orthoscopic and (b) conoscopic images of complex **1**/**4** in a 5:5 molar ratio in the Sm phase at 55 °C.

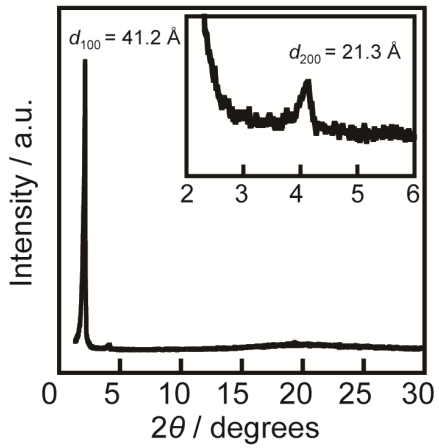

Figure S16. Wide-angle X-ray diffraction pattern of mixture **1**/**4** in a 5:5 molar ratio in the Sm phase at 120 °C.

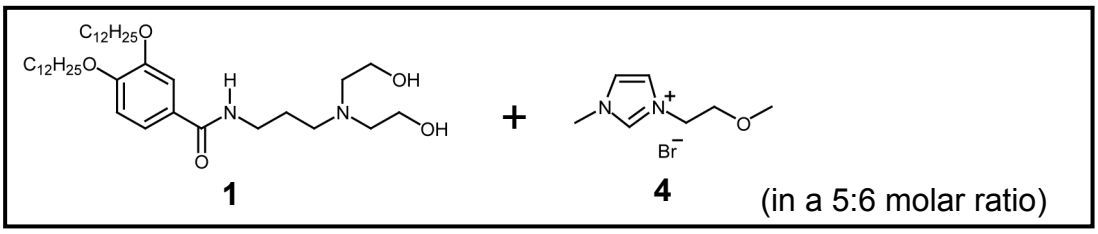

Figure S17. Polarising optical micrograph of mixture **1**/**4** in a 5:6 molar ratio in the Cub_{V1} at 80 °C.

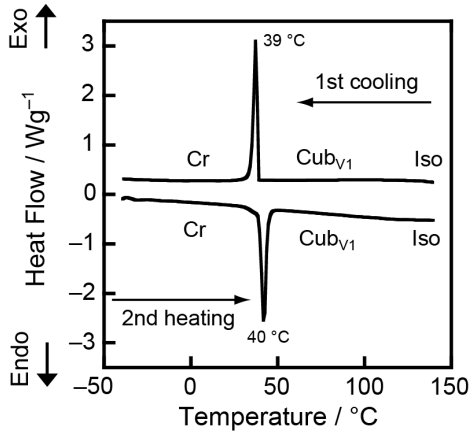

Figure S19. DSC thermograms of mixture **1**/**4** in a 5:6 molar ratio.

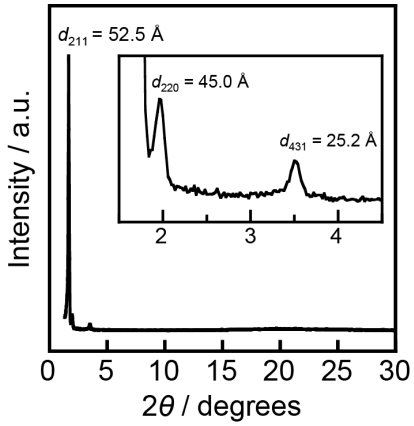

Figure S18. Wide-angle X-ray diffraction pattern of mixture **1**/**4** in a 5:6 molar ratio in the Cub_{V1} at 80 °C.

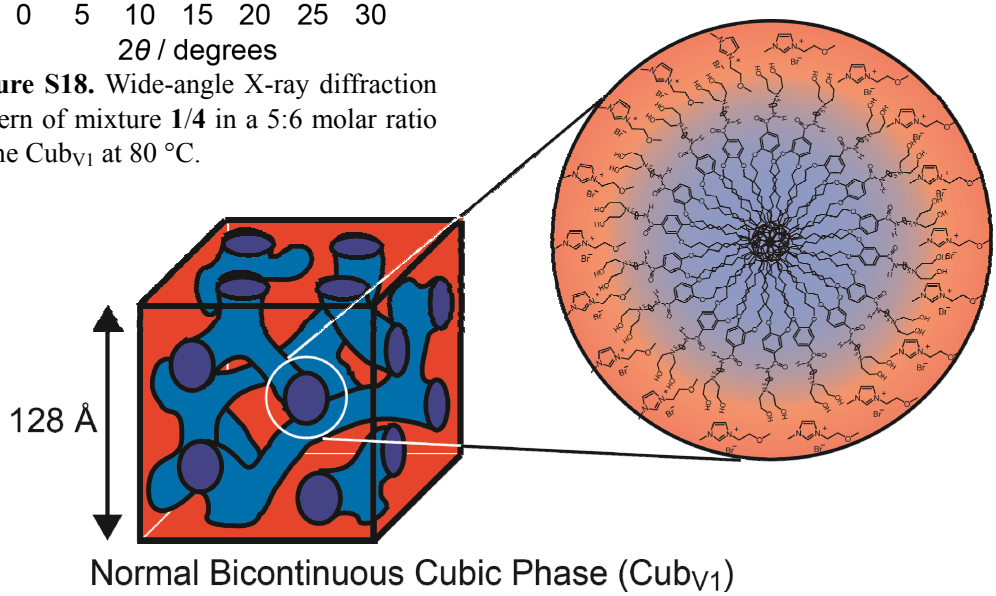

Figure S20. Schematic illustration of the al bicontinuous cubic structure formed by mixture **1**/**4** in a 5:6 molar ratio at 80 °C.

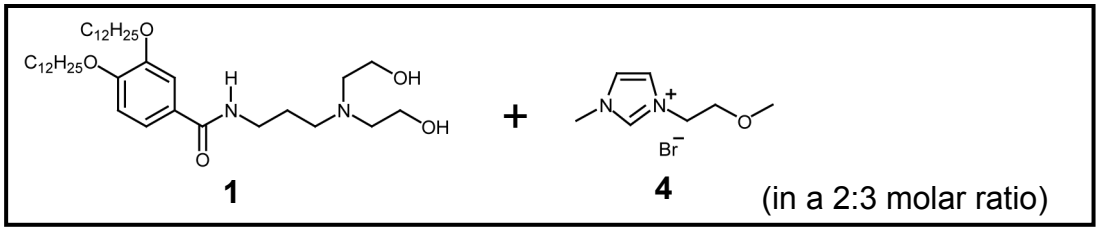

Figure S21. Polarising optical micrograph of mixture **1**/**4** in a 2:3 molar ratio in the Cub_{V1} at 80 °C.

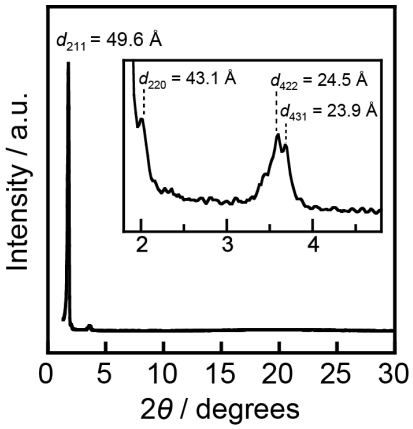

Figure S22. Wide-angle X-ray diffraction pattern of mixture **1**/**4** in a 2:3 molar ratio in the Cub_{V1} at 80 °C.

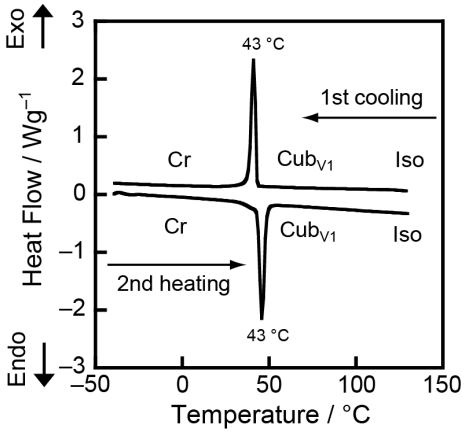

Figure S23. DSC thermograms of mixture **1**/**4** in a 2:3 molar ratio.

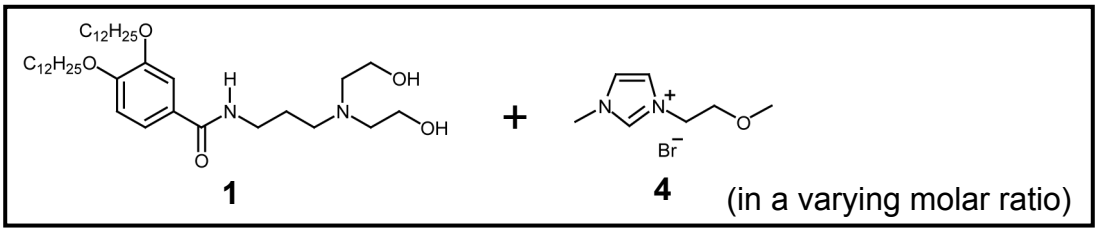

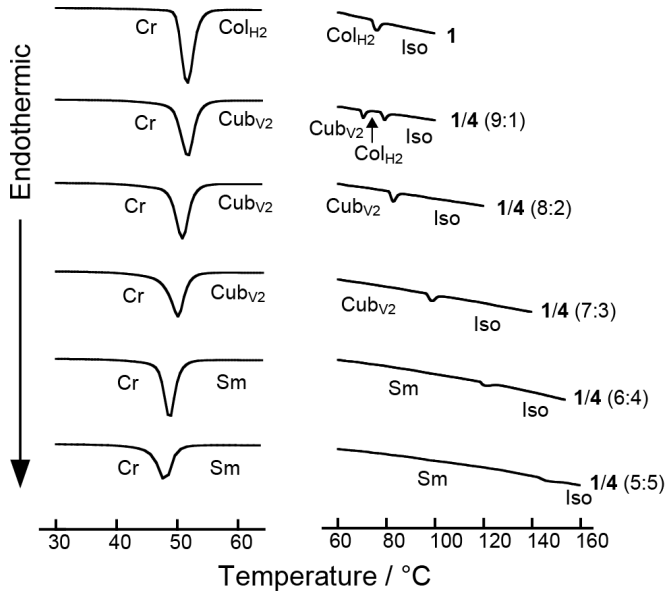

Figure S24. DSC charts of mixtures **1**/**4** containing varying molar fraction of ionic liquid **4** on the second heating process.

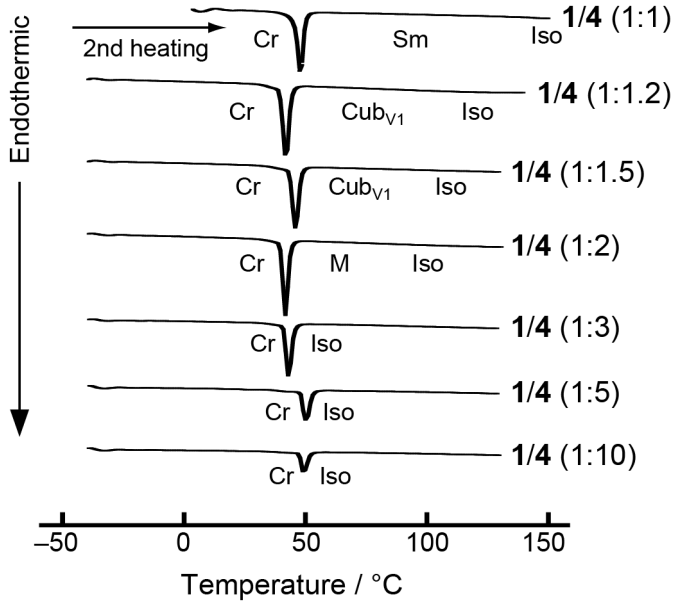

Figure S25. DSC charts of mixtures **1**/**4** containing varying molar fraction of ionic liquid **4** on the second heating process.

4.2. POM, DSC and XRD Results for Mixtures **1**/**5**

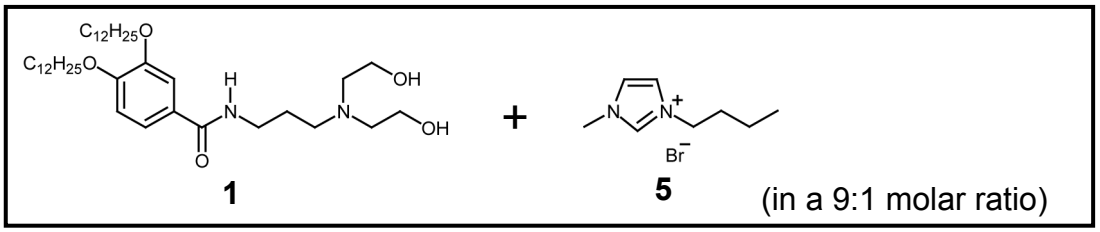

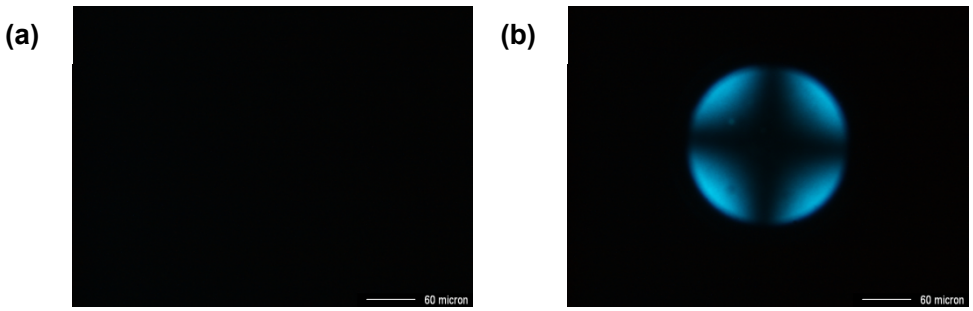

Figure S26. (a) Orthoscopic and (b) conoscopic images of mixture **1**/**5** in a 9:1 molar ratio in the Sm phase at 25 °C.

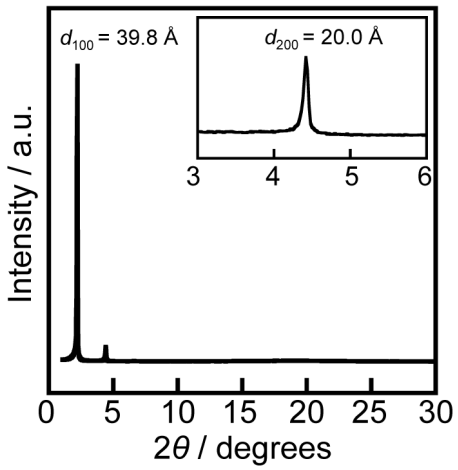

Figure S27. Wide-angle X-ray diffraction pattern of mixture **1**/**5** in a 9:1 molar ratio in the Sm phase at 60 °C.

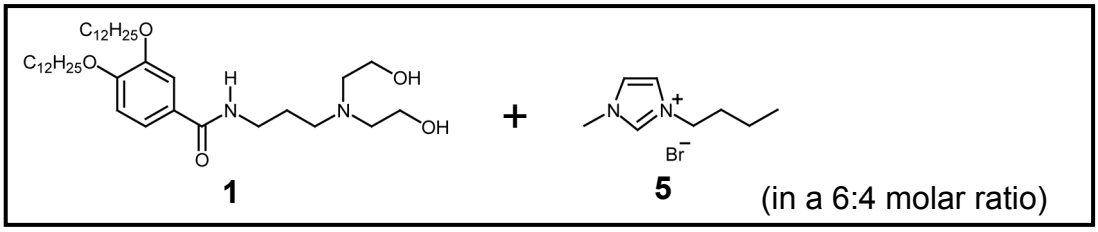

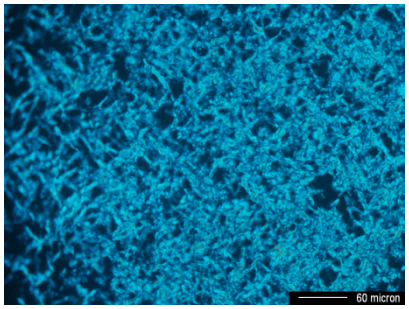

Figure S28. Polarising optical micrograph of mixture **1**/**5** in the molar ratio 6:4 in the Sm phase at 25 °C.

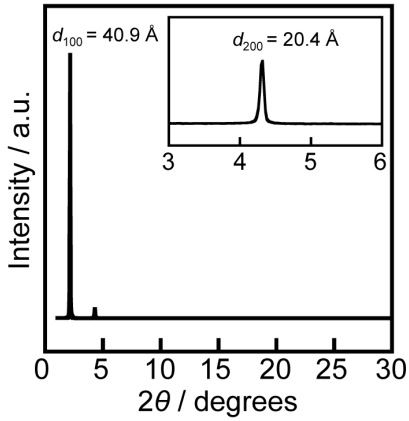

Figure S29. Wide-angle X-ray diffraction pattern of mixture **1**/**5** in the molar ratio 6:4 in the Sm at 100 °C.

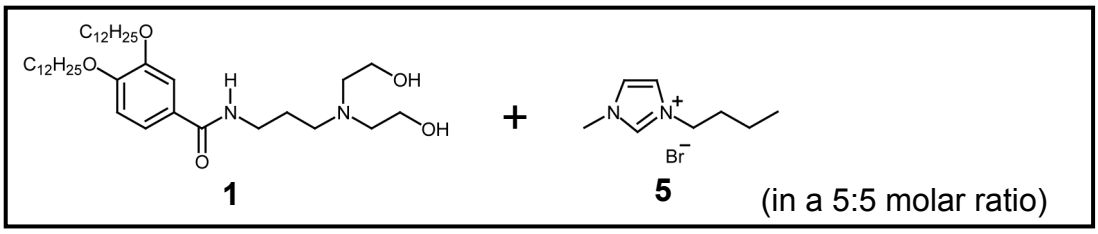

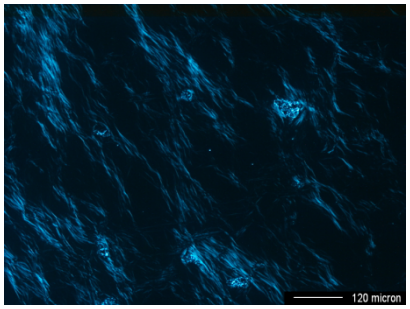

Figure S30. Polarising optical micrograph of mixture **1**/**5** in a 5:5 molar ratio in the Sm phase at 100 °C.

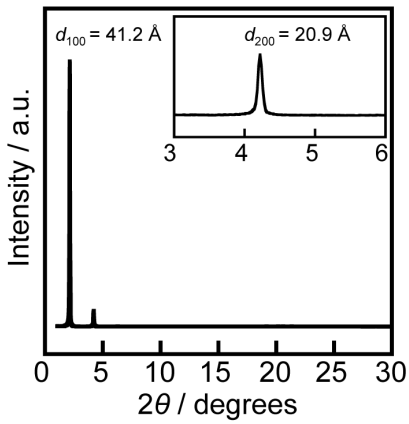

Figure S31. Wide-angle X-ray diffraction pattern of mixture **1**/**5** in a 5:5 molar ratio in the Sm at 100 °C.

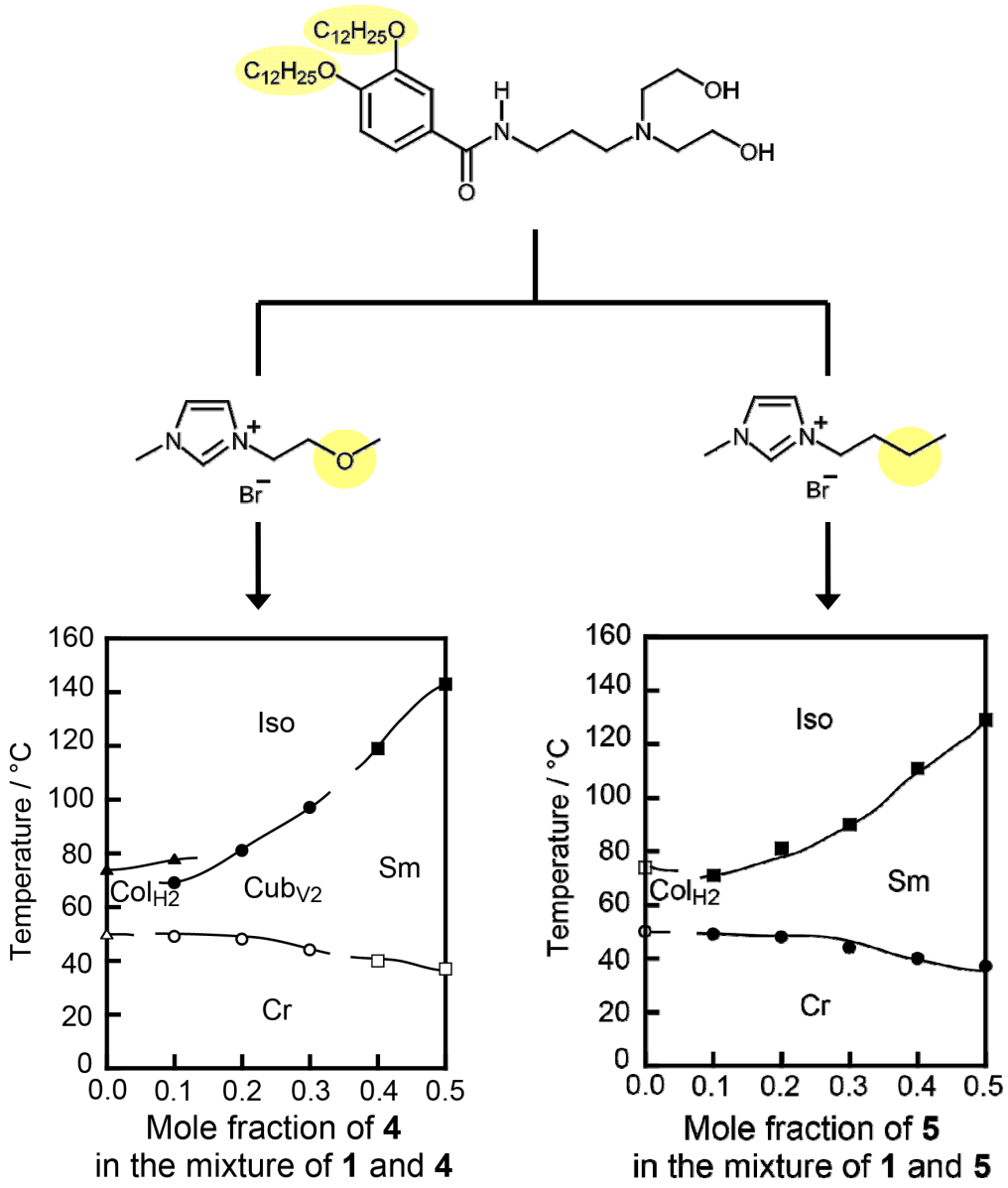

Figure S32. Comparison of the phase diagrams of mixture **1**/**4** and mixture **1**/**5**. The induction of Cub_{V2} phase is exclusively observed for mixture **1**/**4**.

4.3. POM, DSC and XRD Results for Mixtures **2**/**4**

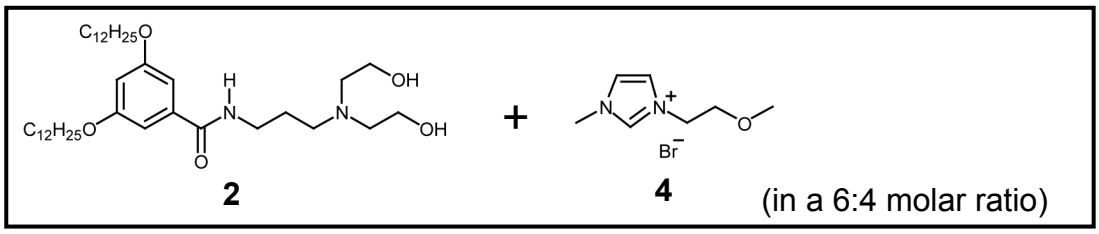

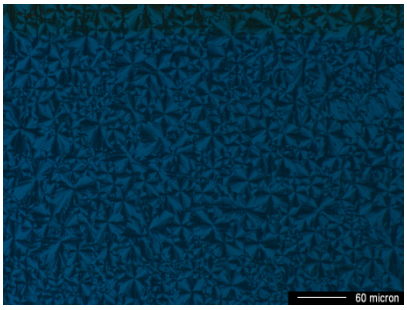

Figure S33. Polarising optical micrograph of mixture **2**/**4** in a 6:4 molar ratio in the Col_{H2} at 25 °C.

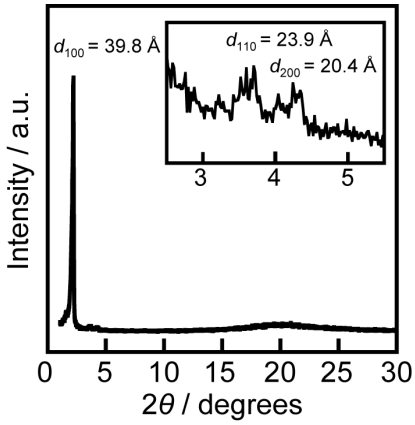

Figure S34. Wide-angle X-ray diffraction pattern of mixture **2**/**4** in a 6:4 molar ratio in the Col_{H2} at 25 °C.

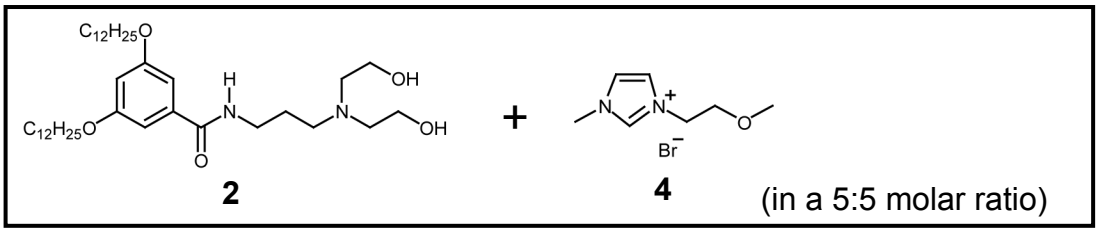

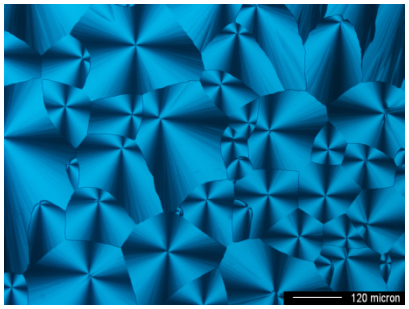

Figure S35. Polarising optical micrograph of mixture **2**/**4** in a 5:5 molar ratio in the Col_{H2} at 45 °C.

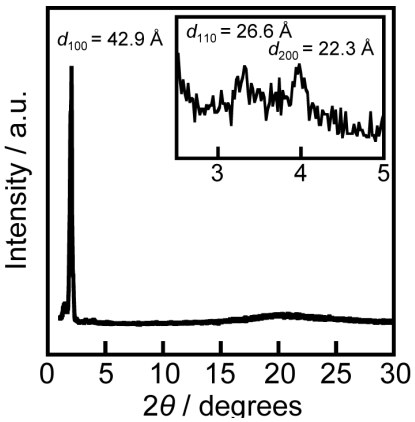

Figure S36. Wide-angle X-ray diffraction pattern of mixture **2**/**4** in a 5:5 molar ratio in the Col_{H2} at 45 °C.

4.4. POM, DSC and XRD Results for Complexes **3**/**4**

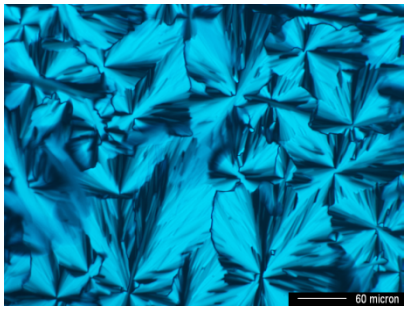

Figure S37. Polarising optical micrograph of mixture **3**/**4** in a 9:1 molar ratio in the Col_{H2} at 50 °C.

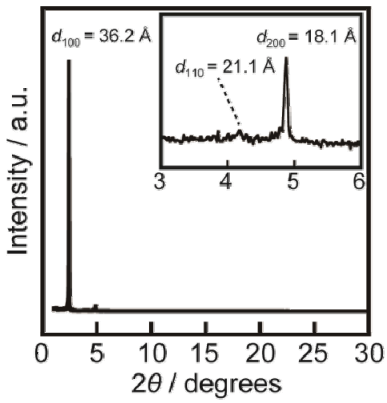

Figure S38. Wide-angle X-ray diffraction pattern of mixture **3**/**4** in a 9:1 molar ratio in the Col_{H2} at 50 °C.

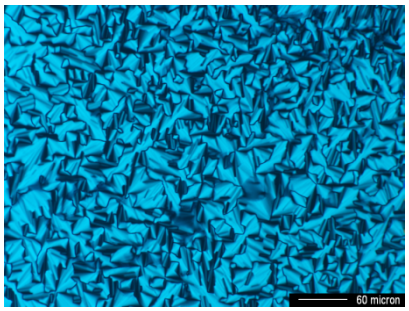

Figure S39. Polarising optical micrograph of mixture **3**/**4** in a 7:3 molar ratio in the Col_{H2} at 80 °C.

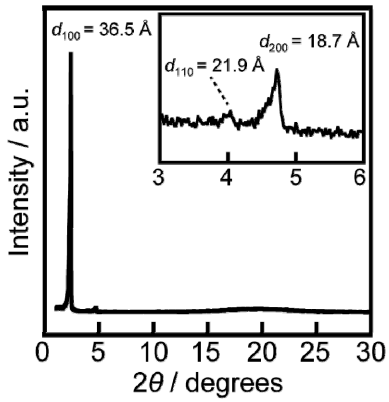

Figure S40. Wide-angle X-ray diffraction pattern of mixture **3**/**4** in a 7:3 molar ratio in the Col_{H2} at 80 °C.

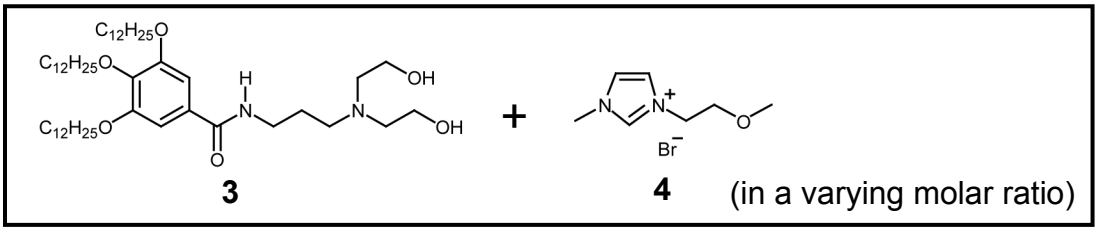

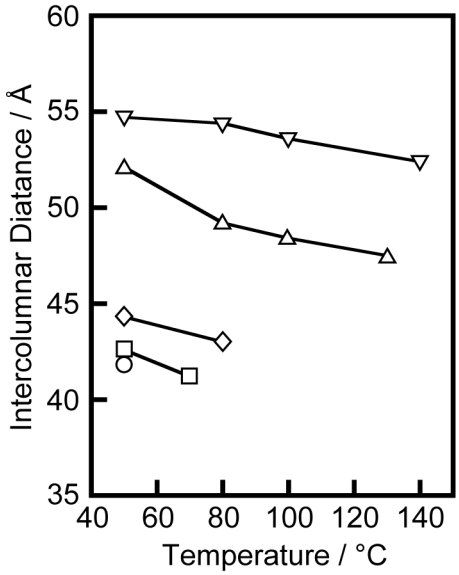

Figure S41. Temperature dependence of intercolumnar distances for mixture **3**/**4** with varying molar ratio in the Col_{H2} phase. Mixture **3**/**4** in the molar ratio of 9:1 (○), 8:2 (□), 7:3 (◇), 6:4 (△), and 5:5 (▽).

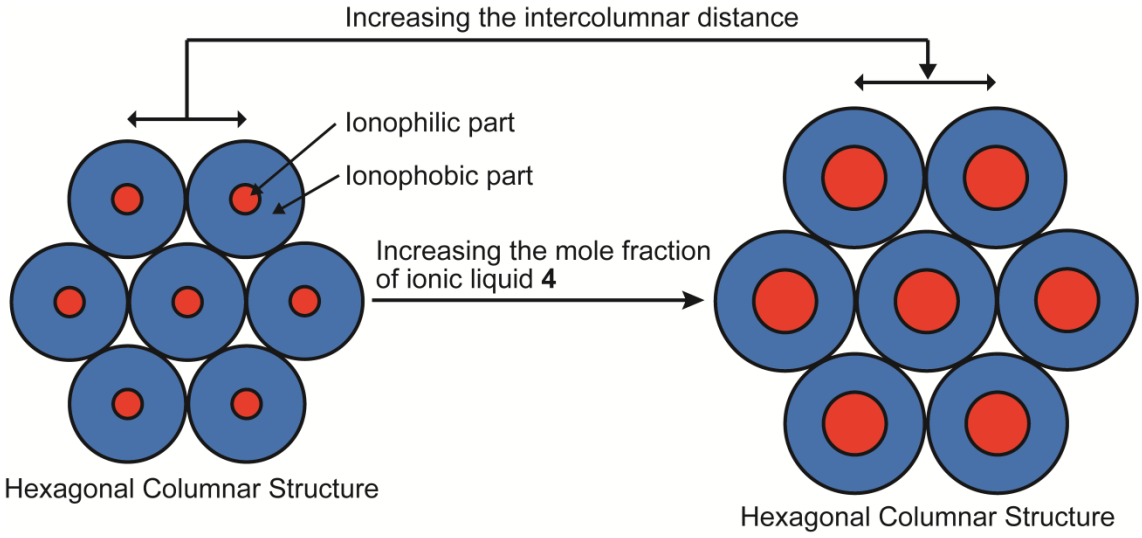

Figure S42. Schematic illustration of the hexagonal columnar structures formed by mixture **3**/**4**. Increasing the mole fraction of ionic liquid **4** in mixture **3**/**4** leads to the increase of the intercolumnar distances.

4.5. Comparison of Mixtures **1**/**4**, **2**/**4**, and **3**/**4**

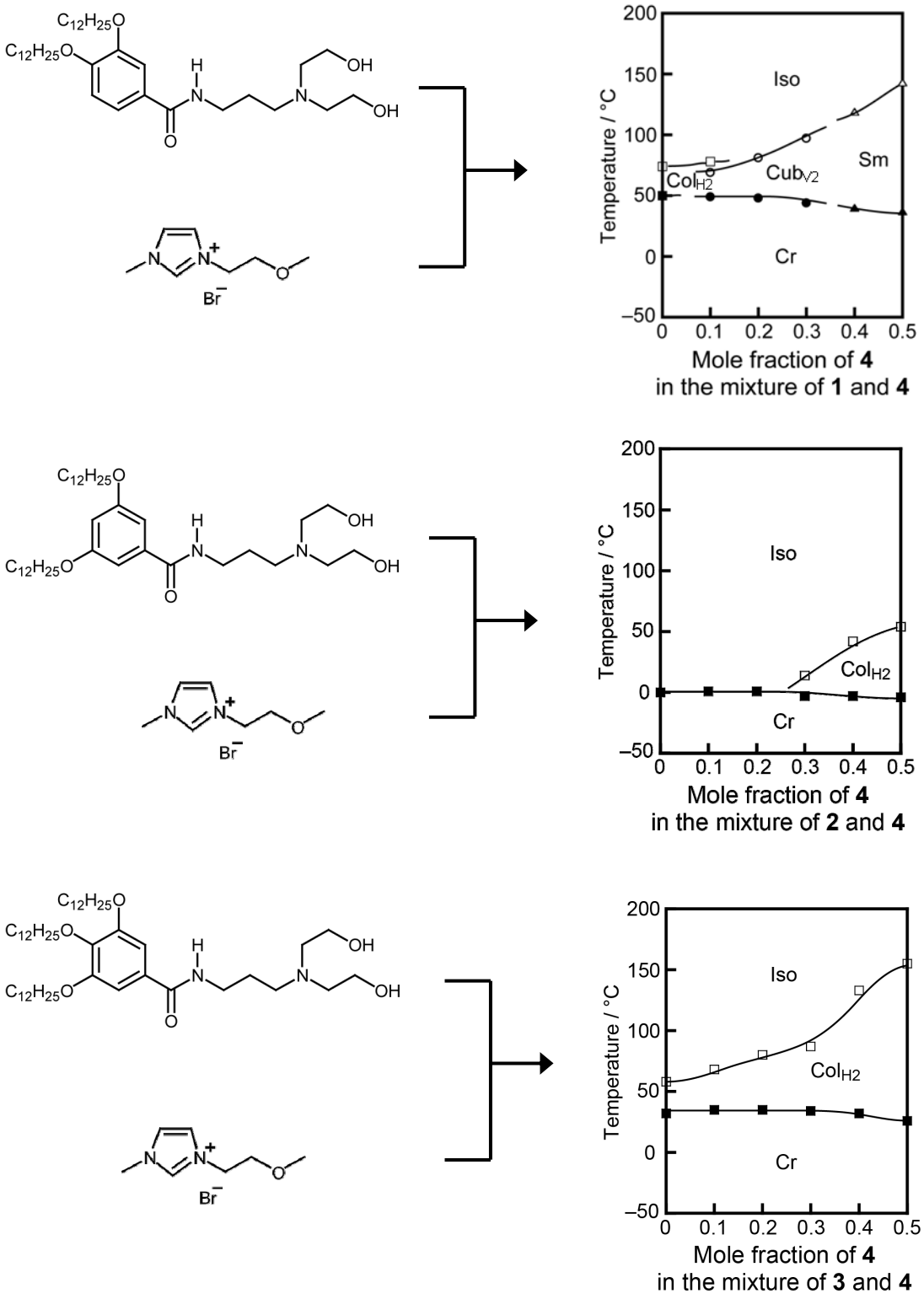

Figure S43. Comparison of phase diagrams for mixtures **1**/**4**, **2**/**4**, and **3**/**4**. The induction of Cub$_{V2}$ phase is observed exclusively for complex **1**/**4**.

4.6. POM, DSC and XRD Results for Complexes **3**/**5**

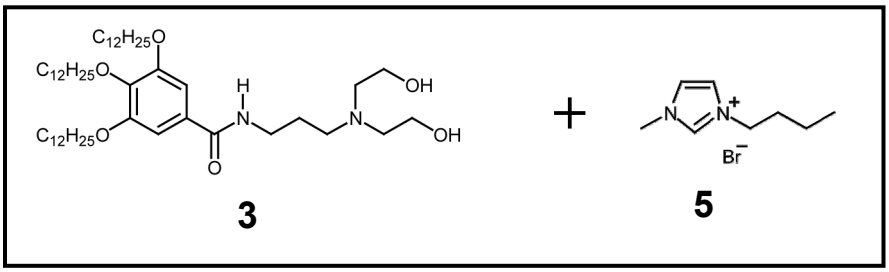

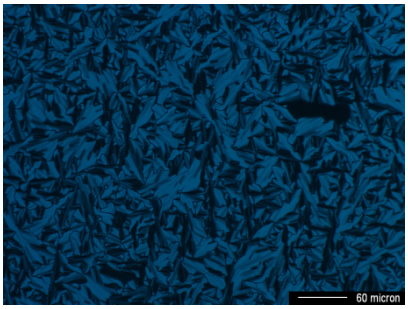

Figure S44. Polarising optical micrograph of mixture **3**/**5** in an 8:2 molar ratio in the Col_{H2} at 50 °C.

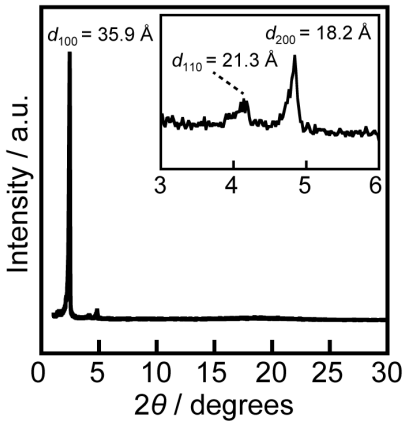

Figure S45. Polarising optical micrograph of mixture **3**/**5** in an 8:2 molar ratio in the Col_{H2} at 50 °C.

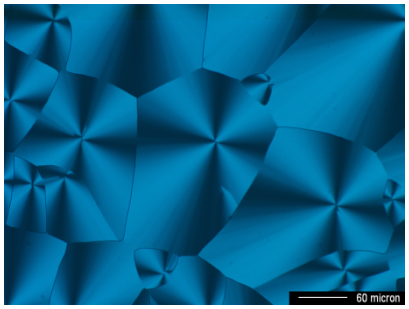

Figure S46. Polarising optical micrograph of mixture **3**/**5** in a 5:5 molar ratio in the Col_{H2} at 100 °C.

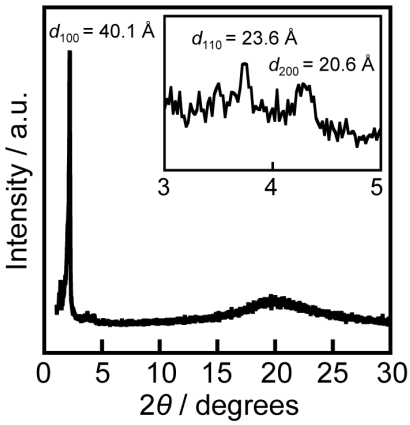

Figure S47. Polarising optical micrograph of mixture **3**/**5** in a 5:5 molar ratio in the Col_{H2} at 100 °C.

4.7. Comparison of Complexes **2**/**4** and **2**/**5**

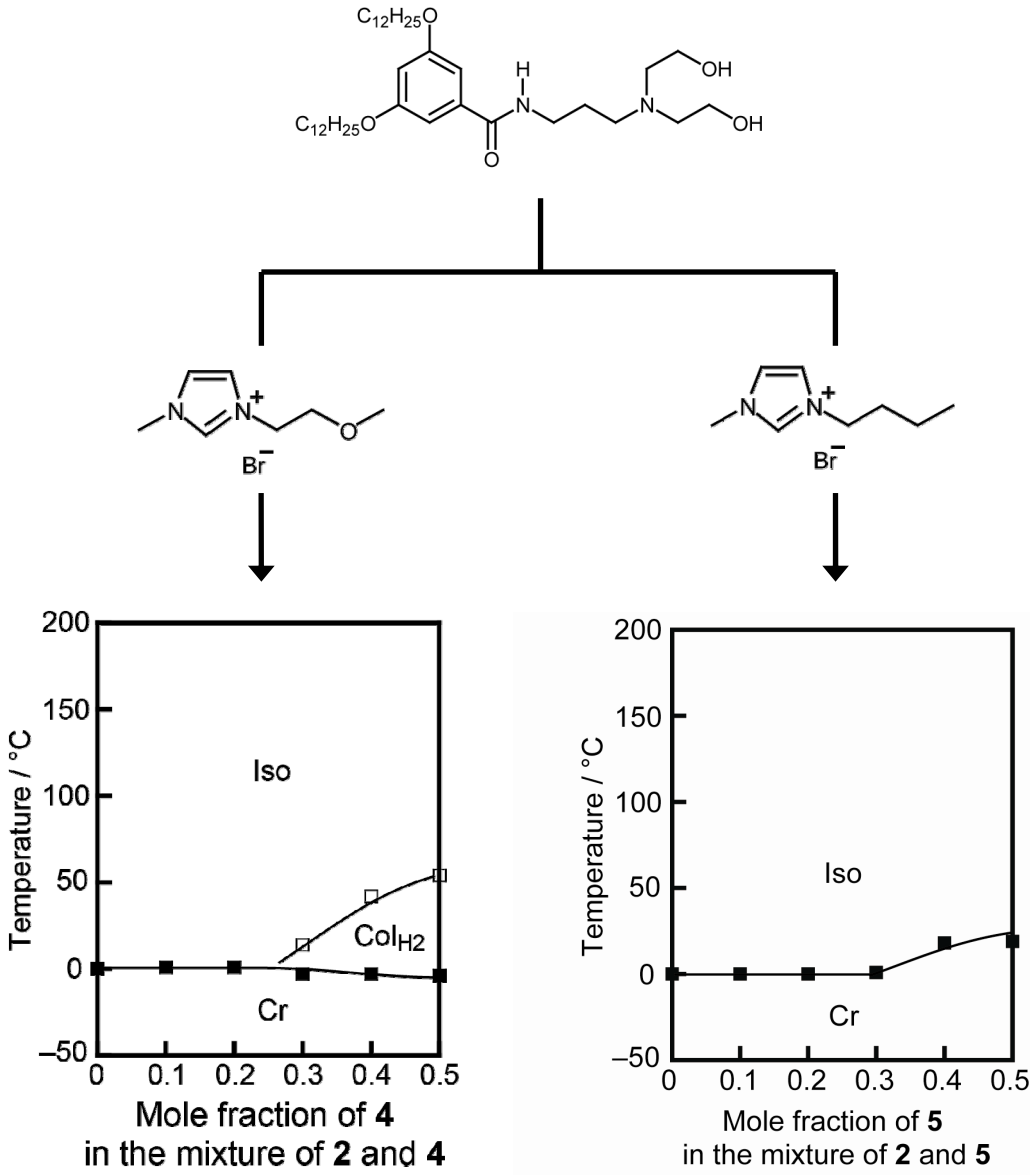

Figure S48. Comparison of the phase diagrams of mixture **2**/**4** and mixture **2**/**5**.

5. NMR study on the Mixtures of Ionic Liquid 4 and Triethanolamine

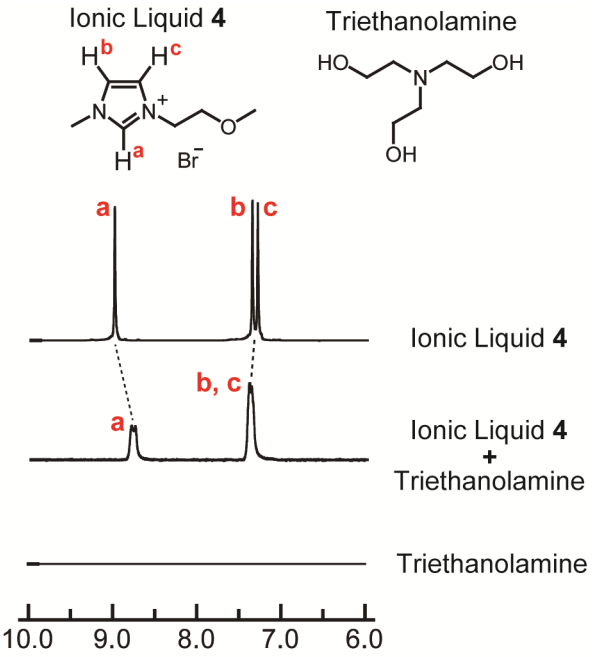

Figure S49. NMR spectra of ionic liquid **4**, triethanolamine, and their mixture in the bulk states at 60 °C. These results were obtained by using coaxial capillary tubes.

6. IR study on Complex 1/4, Compound 1, and Ionic Liquid 4

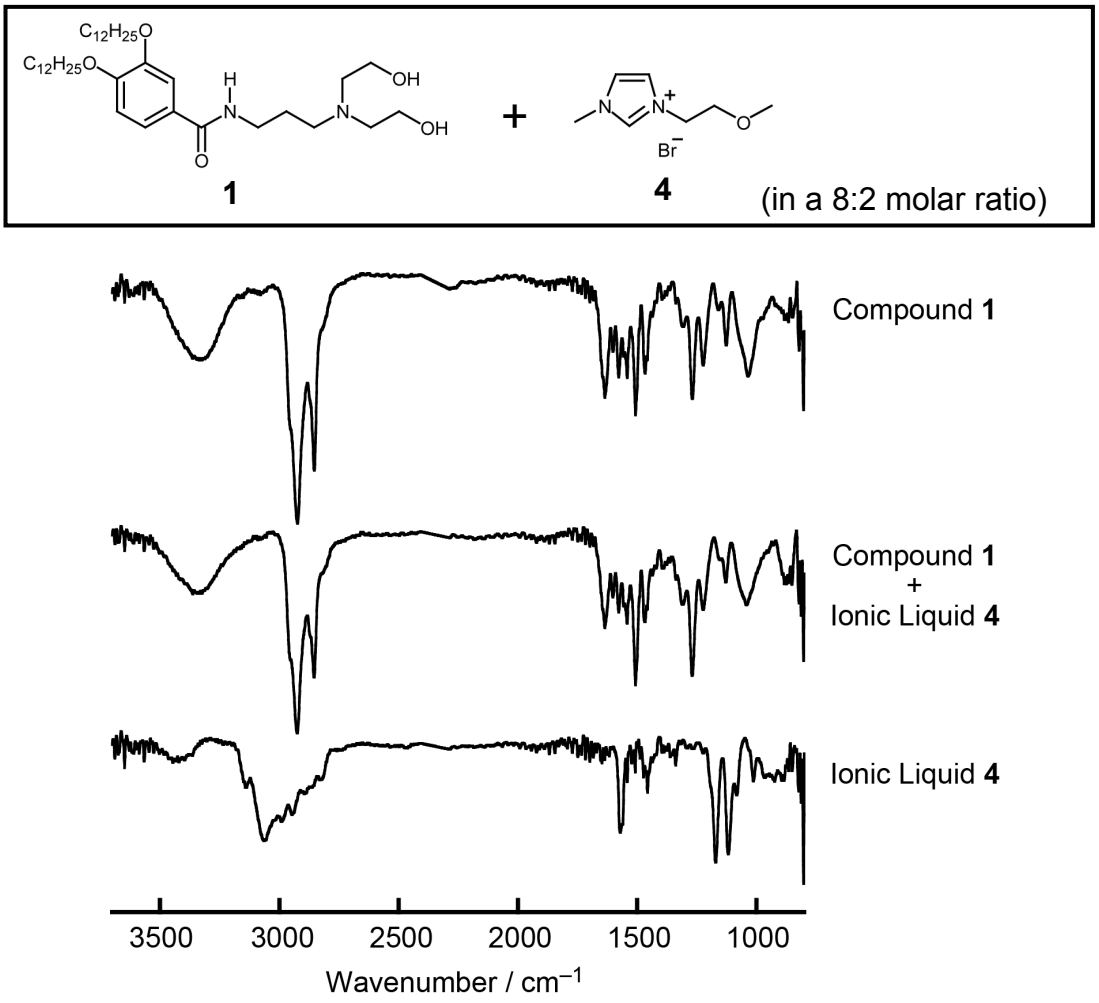

Figure S50. IR spectra of compound **1**, ionic liquid **4** and their mixture at 60 °C.

IR measurements were performed for compound **1**, ionic liquid **4** and their mixture. Figure S50 shows the IR spectra of these materials at 60 °C. The stretching band of the hydroxyl group (ν_{OH}) of compound **1** appears as a broad peak in the region from 3200 to 3500 cm^{-1}. This peak is observed as a broad peak at the same position for mixture **1**/**4**. Due to the broadness of these peaks, it is difficult to discuss the change of ν_{OH} as the addition of ionic liquid **4**. On the other hand, the stretching band of the C-H bonding on the C2 of the imidazolium ring ($\nu_{C2\text{-}H}$) for ionic liquid **4** shows a sharp peak at 1570 cm^{-1} and some peaks in the range of 2800-3000 cm^{-1}. These peaks have a substantial overlap with those of compound **1**. Therefore, it is difficult to the change of $\nu_{C2\text{-}H}$ upon mixing **4** with **1**.

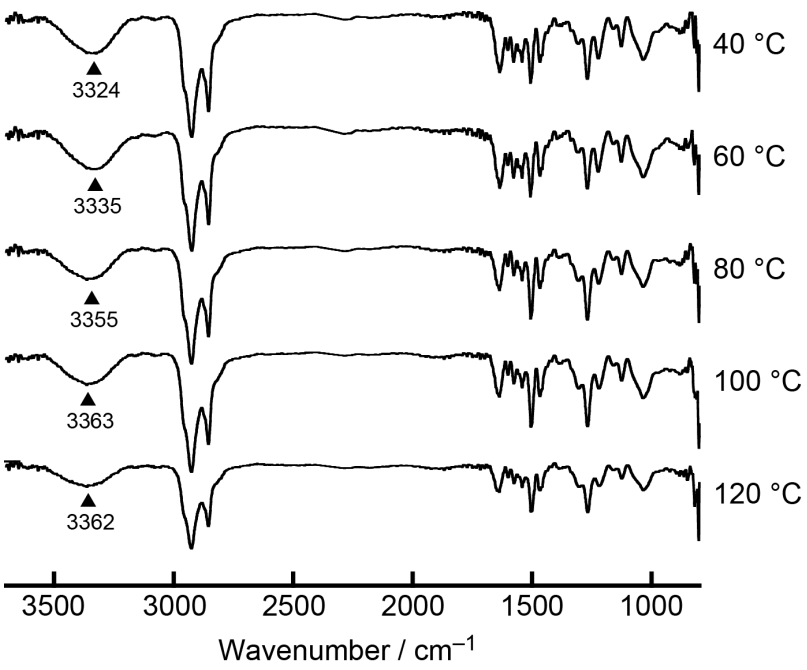

Figure S51. IR spectra of compound **1** at varying temperatures.

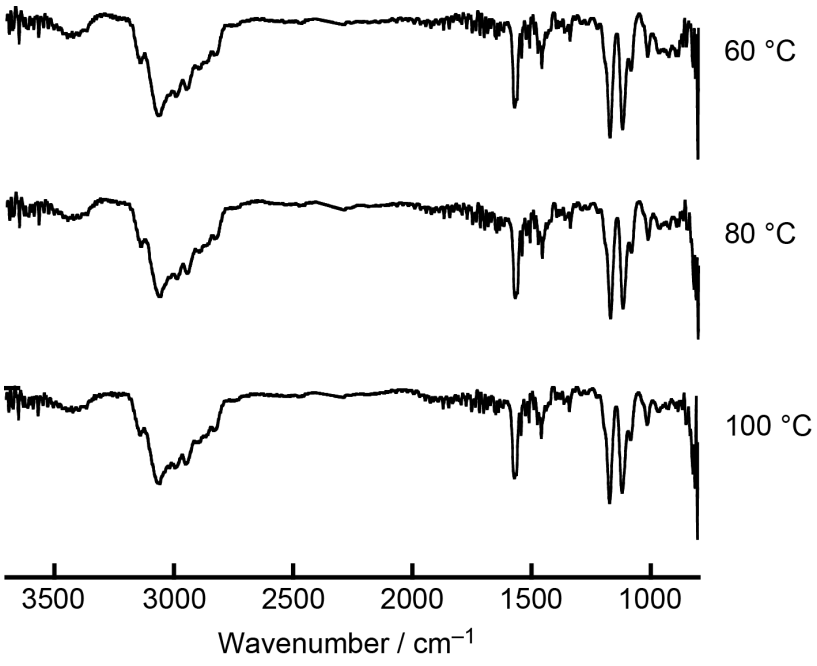

Figure S52. IR spectra of ionic liquid **4** at varying temperatures.